Theoretical description of logical stochastic resonance and its enhancement: Fast Fourier transform filtering method

Dong Yu, Xuan Zhan, Li-jian Yang, and Ya Jia[*]

Department of Physics and Institute of Biophysics, Central China Normal University, Wuhan 430079, China

Over the past decade, dynamic schemes have been proposed for the use of bistable systems in the design of logic devices. A bistable system in a noisy background can operate as a reliable logic gate in a moderate noise level, which is called a logical stochastic resonance (LSR). In this paper, we theoretically explore the emergence of LSR in general bistable systems and identify the dynamical mechanisms of LSR. The timescale relationship between the measured time and the mean first-pass time of two-state transitions is a key condition in determining whether the system is reliable. Furthermore, we demonstrate that the stability of the logic operation can be significantly improved by choosing the appropriate filtering method. Low-pass filtered noise-driven systems are more stable than Gaussian white noise. However, band-pass and high-pass filtered noise are harmful to the stability of the system due to the filtering of low-frequency components. Our theoretical and numerical simulation results offer perspectives for the development of logic devices.

I. INTRODUCTION

The size of logic devices continues to shrink, making it increasingly difficult to suppress noise. Noise affects the stability of logic devices and significantly limits the computing speed of logical computational devices [1]. In recent years, more and more researchers have been working to obtain reliable logic operations. Inspired by stochastic resonance [2–5], Murali *et al.* proposed logical stochastic resonance (LSR) [6], i.e., the reliability of logic gates that can be achieved in a suitable noise intensity window. Based on the seminal work of Murali *et al.*, LSR has been further found in a variety of nonlinear systems such as electrical [7,8], nanomechanical [9], optical [10,11], chemical [12], and biological systems [13–16].

Moreover, LSR has attracted a lot of attention as a potential approach for designing unique logic devices. Besides Gaussian white noise-induced LSR, a wide variety of noise-induced LSR has been investigated [17–20]. The enhancement of the LSR by various effects has also been investigated, such as coupling strength [21–23], parameters [24], chaotic activity [25,26], asymmetry of temperature [27], etc. Recently, the direct implementation of all basic logic operations using a single bistable system driven by nonlinearly transformed input signals has been reported [28]. They suggest that flexible logic gates can be implemented using nonlinear transformations of the inputs in bistable systems. In this context, a theoretical description of the LSR mechanism is urgently needed.

Although numerous previous studies have given the emergence of LSR in different systems based on numerical simulation methods and experimental data, a general theoretical description to help us understand the dynamical

mechanisms of LSR is lacking. Therefore, we would like to address two questions: First, whether there is a general way to explain the stochastic process mechanism of LSR. Second, we wanted to find engineering easy ways to enhance LSR. For the former, we solved analytically for the transition probabilities and mean first pass time (MPFT) using the master equation approach of the two-state model. The results provide an understanding of the dynamical mechanisms of LSR. For the latter, we propose a filtered noise-driven system obtained by the fast Fourier transform (FFT) filtering method. The results show that the system is more stable when driven by low-pass filtered noise. This is beneficial for designing more stable logic devices.

The structure of this paper is as follows: in Sec. II, a generalized model of LSR and its theoretical description are introduced. Similarly, numerical simulation methods for measuring LSRs are given. The main results are presented in section 3, while in section 4, we summarize and discuss the potential implications of our findings.

II. MODEL

For simplicity, consider a one-dimensional dynamical system whose state is described by a variable $x(t)$ that follows dynamics

$$\frac{dx}{dt} = -\frac{dU(x)}{dx} + I_{\text{input}}(t) + \xi(t), \tag{1}$$

where $U(x) = -2x^2 + 5x^4 - bx$ is a quartic potential. $\xi(t)$ is a Gaussian white noise with noise intensity D and zero mean ($\langle \xi(t) \rangle = 0$, $\langle \xi(t)\xi(t') \rangle = 2D\delta(t - t')$). The symmetry, depth, and number of potential wells are determined by bias parameter b. The asymmetry of the local minima is depicted in Fig. 1(a). $I_{\text{input}}(t)$ as a logical input current consists of two aperiodic two-level square waves (e.g., I_1 and I_2), which
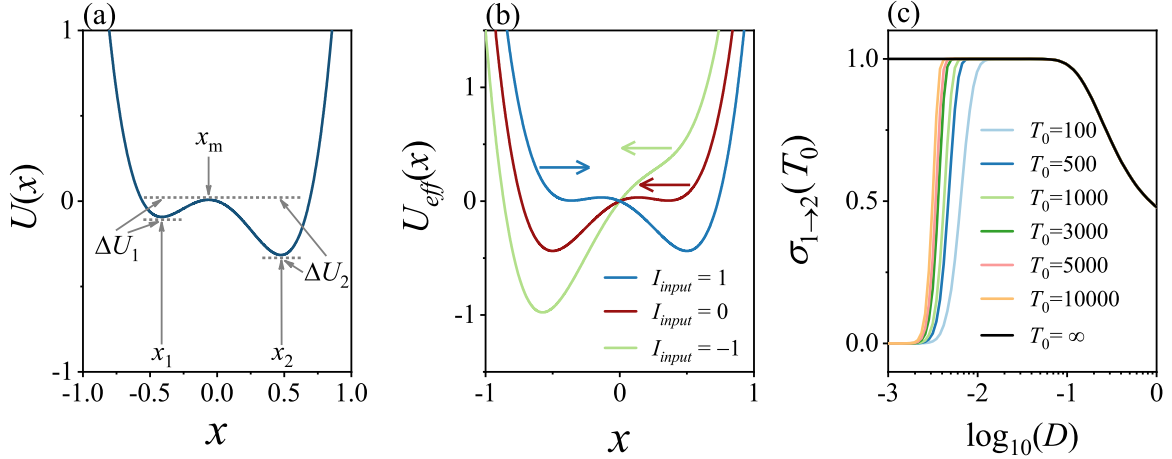
---
*Corresponding author: jiay@ccnu.edu.cn

FIG. 1. (a) Bistable potential $U(x)$ with the asymmetric basin of attractions depicting the positions of the minima x_1 and x_2 and the maximum x_m, and the height of the potential barriers that for this bistable case are ΔU_1 and ΔU_2. (b) Effective potential function $U_{eff}(x)$ under different logic inputs I_{input}, $b = -0.5$ to obtain AND gate. (c) Dependence of the probability $\sigma_{1\rightarrow 2}$ of the system state transition from $x_1 \rightarrow x_2$ on D with different measurement times T_0 (transient process), $I_{input} = 1$. This indicates that the probability of the state transition is influenced by the measurement times T_0.

encode two independent logic inputs. The logical input is 1 if I_1 and I_2 take the value 0.5, and 0 if I_1 and I_2 are -0.5 (Table I). Therefore, four logical input sets of $(0, 0)$, $(0, 1)$, $(1, 0)$, and $(1, 1)$ are obtained by combining two independent logical inputs I_1 and I_2 (Table I). The logical outputs of the system are determined by x. If x is located in the right potential well (i.e., $x > x_m$), the logical output is 1; otherwise, the logical output is 0. Reliable logic operation occurs when the output of the system can be continuously mapped to the logical input. According to previous studies [25], the logic switching between different logic gates can be easily achieved by changing the bias b. In this paper, b is set to -0.5 for AND logical gates and 0.5 for OR logical gates. Alternately, complementary gates (NAND and NOR) can be obtained by interpreting the output as 1 when $x < x_m$, and as 0 when $x > x_m$.

To theoretically solve for the reliability of the logic operation in a noisy background, we obtain the effective potential function $U_{eff}(x, t) = U(x) - I_{input}(t)x = -2x^2 + 5x^4 - (b + I_{input}(t))x$ by incorporating $I_{input}(t)$ into $U(x)$. The properties of U_{eff} are determined by the logical inputs [as shown in Fig. 1(b)]. The system is in the monostable state when $I_{input} = -1$. This allows the system state to always evolve towards the desired logical output. However, when $I_{input} = 1$ and 0, the system is bistable and their potential functions are axisymmetric about $x = 0$. The reliability of the logic operation is governed by the transitions between the asymmetric two potential wells in a noisy background. Therefore, we can solve it analytically using the master equation approach of the two-state model.

First, at a given time t, the state of the system has probability $\sigma_1(t) = P(x(t) < x_m)$ for the left potential well and probability $\sigma_2(t) = P(x(t) > x_m)$ for the right potential well, and $\sigma_1 + \sigma_2 = 1 \forall t$. The initial distribution probability of the system is determined by the initial state of the system: $\sigma_1(0) = P(x(0) < x_m)$ and $\sigma_2(0) = P(x(0) > x_m)$. The master equation for the evolution of the probabilities of these distributions is [29]

$$\frac{d\sigma_1(t)}{dt} = r_2\sigma_2(t) - r_1\sigma_1(t)$$
$$\frac{d\sigma_2(t)}{dt} = r_1\sigma_1(t) - r_2\sigma_2(t), \tag{2}$$

where $r_{1,2}$ is Kramer's escape rate probability, which represents the transition rate out of the $x_{1,2}$ state. It can be calculated by taking the inverse of the analytically obtained MPFT. A rigorous definition of escape time out of x_1 is provided by the MFPT $\langle \Gamma \rangle_{1\rightarrow 2}$ of the process $x(t)$ to reach x_2 with initial condition $x(0) = x_1$. This is given by [30–32]

$$\langle \Gamma \rangle_{1\rightarrow 2} = \int_{x_1}^{x_2} \frac{dx}{DP_{st}(x)} \int_{-\infty}^{x_2} dy P_{st}(y). \tag{3}$$

The term $P_{st}(x)$ is the steady-state distribution function of system. In the case in which the intensity of the noise is small in comparison with the energy barrier, i.e., $D \ll \Delta U(x)$, $\langle \Gamma \rangle_{1\rightarrow 2}$ becomes independent of the initial condition $x(0) < x_m$ and of x_2 [33]. Using the steepest descent approximation, Eq. (3) can

TABLE I. The relationship between the logical inputs and outputs of the basic logic operation of AND and OR gates.

Input signal	Values of I_1 and I_2	Logical I_{input} sets	AND	OR
-1	$(-0.5, -0.5)$	$(0,0)$	$0\ (x < x_m)$	$0\ (x < x_m)$
0	$(-0.5, 0.5)/(0.5, -0.5)$	$(0, 1)/(1, 0)$	$0\ (x < x_m)$	$1\ (x > x_m)$
1	$(0.5, 0.5)$	$(1,1)$	$1\ (x > x_m)$	$1\ (x > x_m)$

be approximated as [34,35]

$$\langle\Gamma\rangle_{1\to2} = 2\pi[|U''(x_1)U''(x_m)|]^{-\frac{1}{2}}\exp\left[\frac{\Delta U_1}{D}\right]$$

$$\langle\Gamma\rangle_{2\to1} = 2\pi[|U''(x_2)U''(x_m)|]^{-\frac{1}{2}}\exp\left[\frac{\Delta U_2}{D}\right]. \qquad (4)$$

The terms ΔU_1 and ΔU_2 are the heights of the potential barriers in the bistable case [as shown in Fig. 1(a)]. Then, one can obtain Kramer's escape rate probability:

$$r_{1,2} = \frac{1}{2\pi}[|U''(x_1)U''(x_m)|]^{\frac{1}{2}}\exp\left[\frac{-\Delta U_{1,2}}{D}\right]. \qquad (5)$$

The analytical solution of Eq. (2) can be easily solved:

$$\sigma_1(t) = \sigma_1(t\to\infty)[1 - \exp(-\nu t)] + \sigma_1(t=0)\exp(-\nu t), \qquad (6)$$

$$\sigma_2(t) = \sigma_2(t\to\infty)[1 - \exp(-\nu t)] + \sigma_2(t=0)\exp(-\nu t), \qquad (7)$$

where $\sigma_1(t\to\infty) = r_2/\nu$ and $\sigma_2(t\to\infty) = r_1/\nu$ are steady-state probability distributions, $\nu = r_1 + r_2$. The state distribution of the system can be solved using distribution probabilities $\sigma_{1,2}$. The reliability of the logic gates depends on whether the states of the system can be continuously mapped to the logic input when the logic input changes dynamically. Therefore, we believe that the logic gate is reliable as the state of the system reaches the desired position within the measurement time T_0.

To numerically quantify the reliability of desired logic output, the success probability P of achieving the desired logic output is calculated for different input sets by the following formula:

$$P = \frac{N_{\text{suc}}}{N_{\text{tot}}}, \qquad (8)$$

where N_{tot} represents the total number of runs and N_{suc} represents the number of successful runs. Here, a successful run means that the outputs of all input sets in this run match the desired logical result. The total number of runs is set to 1000. For each run, the measurement time T_0 is considered to be a transient process, and the calculation time interval $T_{\text{inter}} = 1000$ time units are taken into account in the calculation of P.

The fast response to logical signals is conducive to the speed of computer operation. The system's response speed is characterized by the switching time S. The switching time S is the time that the system takes to switch from low to high states or vice versa after the switching of the input I_{input} occurs. In our simulations, switching times S are calculated during 20 000 consecutive and random I_{input} pulse trains. Smaller switching times indicate faster operation of the logical devices.

For numerical simulations, the improved Euler method with a fixed time step of 0.01 is used to integrate Eq. (1). The Gaussian white noise has been generated using the Box-Muller algorithm [36].

III. RESULTS

A. Theoretical description of LSR

In the above model, one can easily understand the shape and characteristics of the LSR curves previously reported in the literature. As can be seen in Fig. 1(c), the transition probability $\sigma_{1\to2}$ of the desired state transition is determined by the measurement time T_0. Furthermore, our analytical results are in agreement with numerical simulation results. In practice, the logic operation should be completely successful. Therefore, a logical system is reliable when the probability of success for logical operations is approximately equal to 1. For this purpose, we set the data in Fig. 1(c) to 0 for values less than 99.999% and consider the adjusted data as the success probability of the logical operation [analytical results represented by the grey line in Fig. 2(a)].

The results of the analytical solution and numerical simulations lead to quantitatively consistent conclusions: Bistable systems in a noisy background obtain reliable logic operation in the optimum noise intensity window. In addition, the measurement time T_0 (or transient process) increases size L of the optimal noise intensity window and therefore improves the stability of the logic system [as shown in Fig. 3(a)]. Moreover, the numerical simulation results converge with the analytical solution as T_0 increases [the blue dotted line in Fig. 3(a)]. A quantitative comparison between MFPT $\langle\Gamma\rangle_{1\to2}$ and switching times S in Fig. 2(b) also confirms the above conclusions.

Thus, we can understand the dynamical mechanisms of LSR in terms of a two-state evolutionary model. First, in a weak-noise background, the system needs to undergo a long time of evolution to complete the desired transition due to the large first-pass time scale [Fig. 4(a)]. The system is unable to complete the desired transition quickly enough to obtain reliable logic operation within the measurement time T_0. This is why the lower resonance threshold of the LSR is modulated by T_0 in Fig. 3(b). Second, due to the asymmetry of the depth ΔU of the two potential wells, the MFPT of the transitions between the two potential wells in Eq. (4) have different timescales. When D is increased to the window where the MFPT of the desired transition is much less than T_0 and the MFPT of the undesired transition is much greater than T_0, we can obtain reliable logic operations [Figs. 4(b) and 4(c)]. For example, when $D = 0.02$, $\langle\Gamma\rangle_{1\to2} = 23.6$ and $\langle\Gamma\rangle_{2\to1} = 1.82\times10^{10}$. Finally, further increasing D causes the MFPT of the undesired transition to be less than T_0, so we can observe repeated transitions of the system state [Fig. 4(d)].

This can be further verified in Fig. 5. As shown in Fig. 5(a), I_{input} and b determine the stable points $x_{1,2}$ and the unstable point x_m, which also affect the height of the potential barrier (this can be presumed from the difference between $x_{1,2}$ and x_m). Therefore, the MPFT of the steady-state transitions in Eq. (4) is modulated by I_{input} and b. In Fig. 1(b), the transition from x_1 to x_2 is the state transition that matches the desired logic output (the correct transition) and, conversely, the transitions from x_2 to x_1 are the error transitions. Stable and reliable logic operation means that the system completes the correct transitions before measurement time T_0 and does not complete the error transitions for the entire calculation time interval T_{inter}. Therefore, in Fig. 5(b), for the fixed $T_0 = 100$ and $T_{\text{inter}} = 1000$, the increase in the success probability is
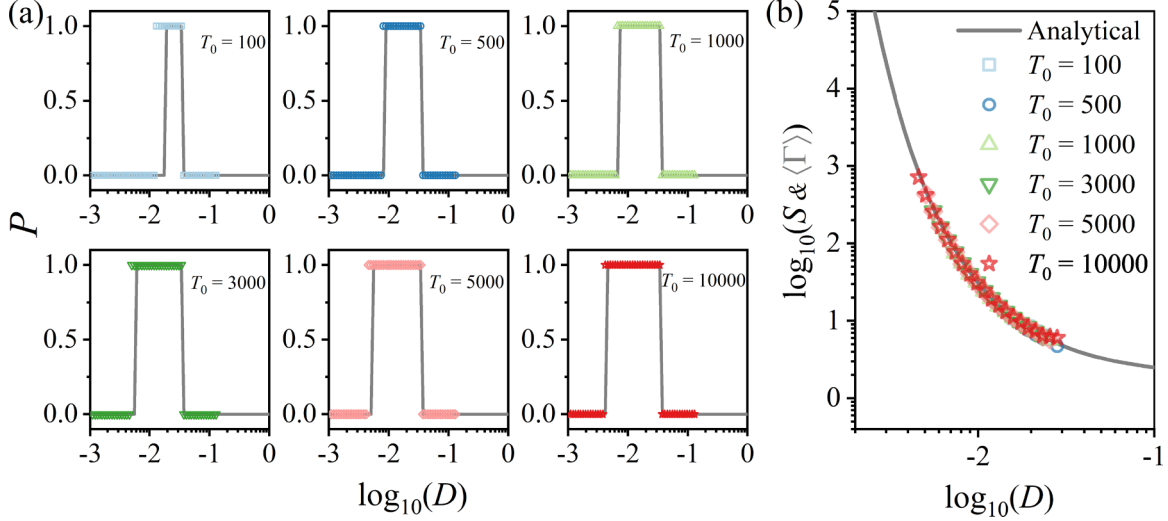
FIG. 2. (a) LSR curves and (b) switching time S obtained in numerical simulations (open circles) compared with transition probability $\sigma_{1 \to 2}$ and MFPT $\langle \Gamma \rangle$ obtained in analytical results (grey line) with different measurement times T_0 (transient process).

determined by the timescale relationship between $\langle \Gamma \rangle_{\text{correct}}$ and T_0. The decrease in the success probability is governed by the timescale relationship between $\langle \Gamma \rangle_{\text{error}}$ and T_{inter}. Only if $\langle \Gamma \rangle_{\text{correct}}$ is much smaller than T_0 and $\langle \Gamma \rangle_{\text{error}}$ is much larger than T_{inter}, the system obtains reliable logical operation. The timescale relationship between the measurement, calculation time, and MFPT of two-state transitions is a key condition in determining whether the system is reliable.

The role of b and I_{input} is to influence the properties of the effective potential well and thus the MFPT. The timescale relationship between the MFPT and the measurement time governs the reliability of the logic operation. So far, we have identified the dynamical mechanisms of b, I_{input}, and noise on the regulation of success probability P. We further explore the method to enhance LSR next. For simplicity, without loss of generality, we fix $b = -|I_{1,2}| = -0.5$ for the AND gate.

B. Enhancement of LSR by filtered noise

In this section, we report a way to drive LSR, where the output of a filtered noise-driven bistable system can be consecutively mapped to a specific logic gate operation. The detailed procedure is as follows:

First, Gaussian white noise is considered as the noise source, to which we apply the FFT filter method to obtain the filtered noise $\xi_f(t)$. The frequency band f_{band} of the $\xi_f(t)$ is determined by the upper f_{max} and lower f_{min} cutoff frequencies. The spectral information of the Gaussian white noise (noise sources) and the filtered noise can be verified in Fig. 6. The corresponding time samples of the time domain filtered noise $\xi_f(t)$ are also given in the inserted subplot for reference.

Second, note that the amplitude (i.e., variance) of the $\xi_f(t)$ is both determined by the frequency bandwidth $\Delta f = f_{\text{max}} - f_{\text{min}}$ and noise intensity D. It is important to independently
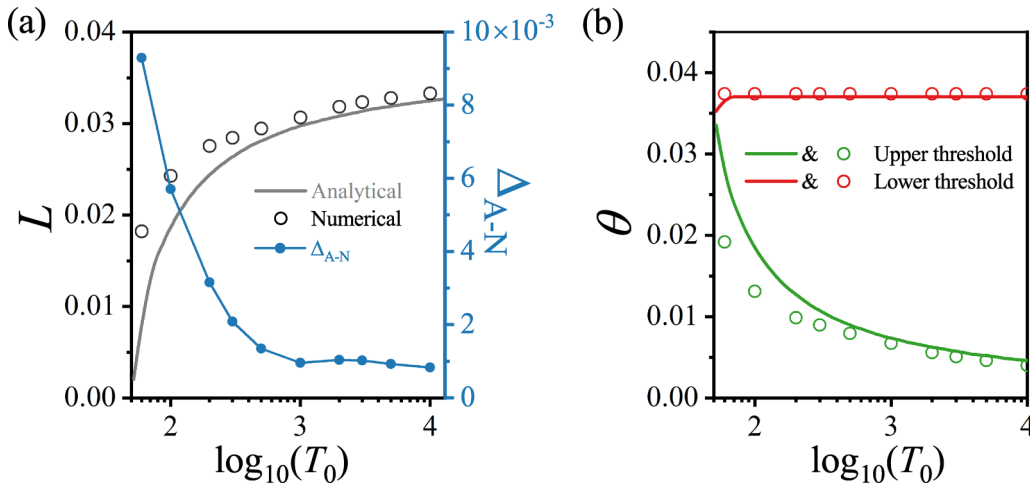

FIG. 3. (a) Dependence of the size L of the optimal window (where $P = 1$) of the noise intensity D on the measurement times T_0. (b) Dependence of the upper and lower resonance threshold θ LSR on T_0. The open circles are the numerical results and the solid lines are the analytical results. The blue dotted line in (a) shows the deviation $\Delta_{\text{A-N}}$ between numerical and analytical results. The figure shows that the agreement between the reported theoretical expressions and numerical simulations increases as T_0 increases.
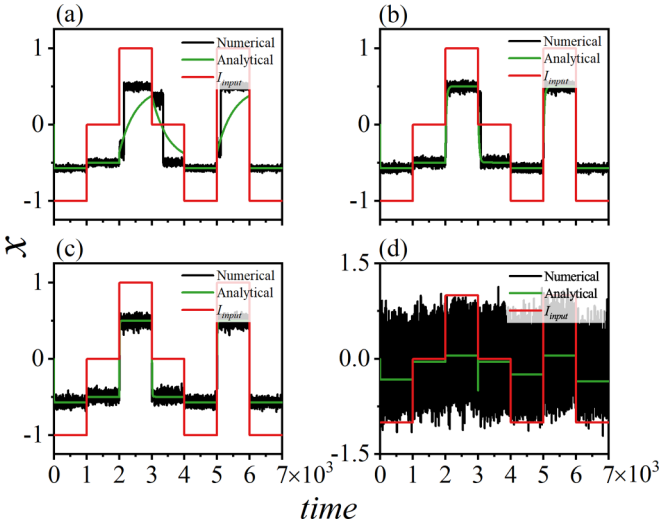
FIG. 4. The sampled time series of the output in numerical (black lines) and analytical (green lines) terms and I_{input} (red lines) for AND logic operations. (a) $D = 0.005$, (b) $D = 0.01$, (c) $D = 0.02$, (d) $D = 1$. The analytical result is estimated by the average state of the system at each time t: $\langle x \rangle_t = x_1 \sigma_1(t) + x_2 \sigma_2(t)$.

analyze the modulation of the frequency domain properties and the fluctuations intensity (i.e., variance) of noise on the LSR. For this reason, it is desirable to coordinate the variance of the $\xi_f(t)$ to be independent of Δf and consistent with the noise source. Therefore, we calculate the variance s^2 and s_{FN}^2 of the source and filtered noise first.

In our paper, the noise source is discrete Gaussian white noise, whose bilateral power spectral density is assumed to be a constant $n_0/2$. The bandwidth of the noise source in the frequency domain is $W = f_s = 1/h$, where f_s is the sampling frequency and h is the integration step. Therefore, the average power of the noise source is $\langle \Upsilon \rangle = f_s n_0/2$. The autocorrelation function $R(\tau)$ and the autocovariance function $C(\tau)$ for Gaussian white noise is

$$
\begin{aligned}
R(\tau) &= \langle \xi(t)\xi(t+\tau) \rangle \\
C(\tau) &= \langle [\xi(t) - m_\xi(t)][\xi(t+\tau) - m_\xi(t+\tau)] \rangle \quad (9) \\
&= \langle \xi(t)\xi(t+\tau) \rangle - m_\xi(t+\tau)m_\xi(t),
\end{aligned}
$$

where $m_\xi(t)$ denotes the mean value function of the stochastic variable $\xi(t)$. When the correlation time τ is 0, the autocorrelation and autocovariance function equal to the average power:

$$
R(0) = \langle \xi(t)^2 \rangle = \langle \Upsilon \rangle C(0) = \langle \xi(t)^2 \rangle - m_\xi(t)^2 = s^2. \quad (10)
$$

Since the mean value function of Gaussian white noise is 0, the variance of the noise source $s^2 = \langle \Upsilon \rangle = f_s n_0/2$. For filtered noise, we set the transfer function:

$$
H(f) = \begin{cases} 1, & f_{min} < |f| < f_{max} \\ 0, & other. \end{cases} \quad (11)
$$

Thus, the power spectral density function of the filtered noise is

$$
S(f) = \begin{cases} \dfrac{n_0}{2}, & f_{min} < |f| < f_{max} \\ 0, & other, \end{cases} \quad (12)
$$

where f_{min} and f_{max} are the upper and lower cutoff frequencies of the filtered noise. Thus, the central frequency $f_c = (f_{min} + f_{max})/2$ and the bandwidth $\Delta f = f_{max} - f_{min}$ can be obtained. According to the Wiener-Khinchin theorem, the autocorrelation function of the filtered noise can be obtained as follows:

$$
R(\tau) = n_0 \Delta f \frac{\sin(2\pi f_c \tau)}{2\pi f_c \tau} \cos(2\pi f_c \tau), \quad (13)
$$

when $\tau \to 0$,

$$
R(\tau \to 0) = n_0 \Delta f \lim_{\tau \to 0} \frac{\sin(2\pi f_c \tau)}{2\pi f_c \tau} \cos(2\pi f_c \tau) = n_0 \Delta f. \quad (14)
$$

Similar to Eqs. (9) and (10), we can obtain the variance of the filtered noise $s_{FN}^2 = n_0 \Delta f$. Thus, the change in variance after filtering is

$$
s_{FN}^2 = \frac{2\Delta f}{f_s} s^2. \quad (15)
$$

The variance of the filtered noise is $2\Delta f/f_s$ times that of the noise source; we can coordinate the intensity of the filtered noise so it is consistent with the variance of the noise source:

$$
D = \frac{f_s}{2\Delta f} D_{eff}. \quad (16)
$$

Equation (16) implies that the filtered noise obtained by the FFT filtering method using a noise source with noise intensity D yields the same variance as that of a noise source with noise intensity D_{eff}. The effective noise intensity D_{eff} is independent of the frequency bandwidth, which offers the possibility to analyze the variance and frequency domain properties of filtered noise individually.

Finally, we use the filtered noise after coordinating the variance to replace the noise term in Eq. (1) as the driving force for the logic operation. Subsequently, numerical simulations are used to investigate the effect of filtered noise on LSR.

The responses of the filtered noise-driven system to the logical input are shown in Fig. 7. By scrutinizing the times series of inputs and outputs, it is clear that the logic device obtains the correct logical output in a particular frequency band f_{band} when the noise intensity D_{eff} is fixed. Therefore, the reliability of the logic operation is strongly modulated by the f_{band}. This indicates that the reliability of logic operations depends on the cooperative effect of the intensity D_{eff} and frequency band f_{band} of filtered noise.

Furthermore, we calculate and show successful probability P in Fig. 8(a) for increasing D_{eff}. The successful probability P shows an abrupt transition from $P = 0$ to the maximum value $P = 1$ with the increase of D_{eff}, and then P decreases to 0 if an increasing D_{eff} exceeds a certain threshold. The successful probability P shows a bell-shaped dependence on the intensity D_{eff} of the filtered noise. The conventional LSR is observed, and its occurrence is due to the filtered noise. The
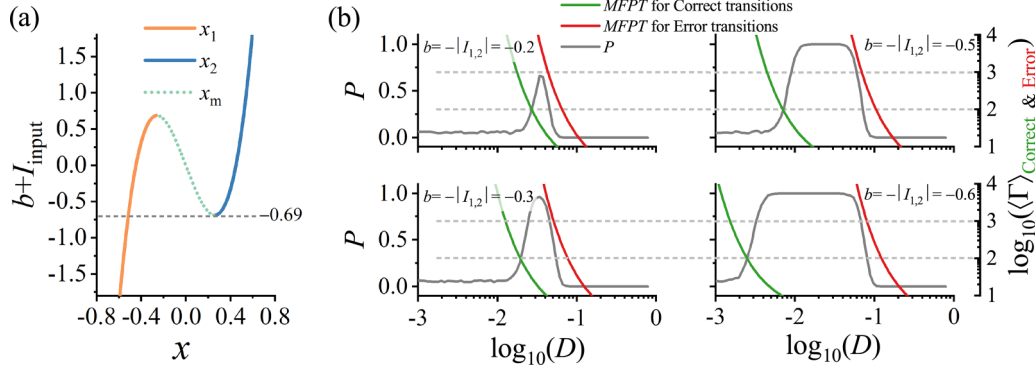
FIG. 5. (a) Bifurcation diagram of x and $b + I_{\text{input}}$ obtained by $dx/dy = -dU_{\text{eff}}(x)/dx$. The solid lines represent stable points and the dashed lines represent unstable ones. (b) Moderation of MFPT $\langle \Gamma \rangle$ on the success probability P. The correct transitions are defined as the state transitions that match the desired logic output; the error transitions are the opposite. The former timescale reduction improves the reliability of logical operations, while the latter impairs the reliability.

switching time S is used as a measure of the speed of the logic operation. In Fig. 8(b), S as a function of D_{eff} is decreasing overall while ensuring correct logic operation. Therefore, the response speed of the logic devices can be improved by appropriate intensity D_{eff} of the filtered noise without destroying its reliability.

To get a global view of how filtered noise affects the reliability of the logic operation, Figs. 9(a)–9(c) show contour plots of the success probability P in the $f_c - D_{\text{eff}}$ plane for band-pass filtered noise, $f_{\text{max}} - D_{\text{eff}}$ plane for low-pass filtered noise and $f_{\text{min}} - D_{\text{eff}}$ plane for band-pass filtered noise, respectively. The output of the system can be continuously mapped to the logic gate operation when the filtered noise is in the parameter range of the black island. This further confirms that the reliability of the logic operation is modulated by the cooperative effect of the intensity and frequency band of filtered noise. However, in a practical system, the variance of the noise (intensity of filtered noise) is not a fixed value and fluctuates within a certain range. Therefore, the range of noise windows over which logic operates reliably is also an important indicator of the stability of logic devices. The stability factor ρ for logical operations is defined as

$$\rho = \frac{\theta_u}{\theta_l}. \tag{17}$$

The upper θ_u and lower θ_l thresholds are the maximum and minimum values of the optimal noise window for LSR, respectively. The dependence of ρ on frequency for the three types of filtered noise is shown in Fig. 9(d). The stability characteristic curve of the band-pass filtered noise [blue line in Fig. 9(d)] shows that the system has lower stability driven by high-frequency filtered noise than by low-frequency filtered noise. Furthermore, the stability is lower than the noise source in all cases except for the first point ($f_{\text{band}} = 0 - 1$). Therefore, the band-pass filtering method is not an optimal choice. By the same token, the high-pass filtering method is not superior [green line in Fig. 9(d)]. Further analysis of these two characteristic curves reveals that the disappearance of the low-frequency band damages the stability of the logic operation. In contrast, for the case of low-pass filtered noise [red line in Fig. 9(d)], the system obtains higher stability when the higher frequency bands are filtered. The more high-frequency bands are filtered, the stronger the stability of the system's logic operation.

In addition, there is a limit to the behavior that enhances the stability of logic operations by filtering higher frequency bands noise. As shown in Fig. 10, when the upper cutoff frequency is very small ($f_{\text{max}} < 0.03$), the system is unable to perform reliable logic operations under any noise window. The stability characteristic curve of the system [Fig. 10(b)] shows a bell-shaped dependence on f_{max}. Therefore, there is an optimal low-pass filtering method that makes the system most stable. As can be observed in Fig. 10(a), the resonance threshold is minimal at this point. This further demonstrates that the low-pass filtering method is a superior way to improve the stability of the system's logic operation while reducing the intensity of the required drive.
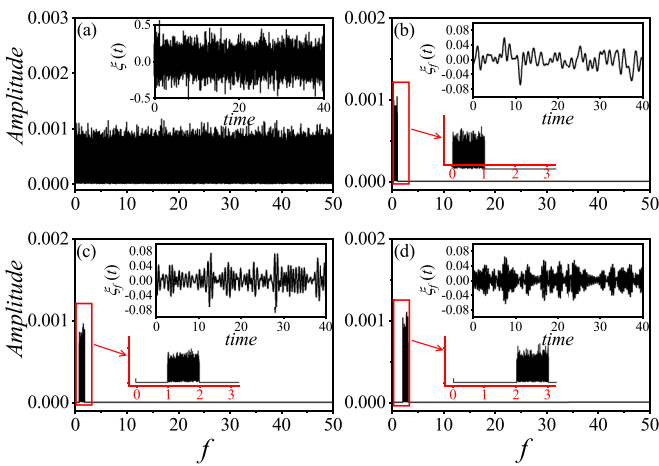

FIG. 6. (a) Schematic representation of the filtering method. (b1) Spectrum of noise sources $\xi(t)$ after FFT. The spectrum of the filtered noise $\xi_f(t)$ after the FFT with the frequency bands: (b2) $f_{\text{band}} = 0 \sim 1$ (i.e., $f_{\text{min}} = 0$, $f_{\text{max}} = 1$); (b3) $f_{\text{band}} = 1 \sim 2$ (i.e., $f_{\text{min}} = 1$, $f_{\text{max}} = 2$); (b4) $f_{\text{band}} = 2 \sim 3$ (i.e., $f_{\text{min}} = 1$, $f_{\text{max}} = 2$). The inserted subplot shows the time evolution of $\xi(t)$ and $\xi_f(t)$.
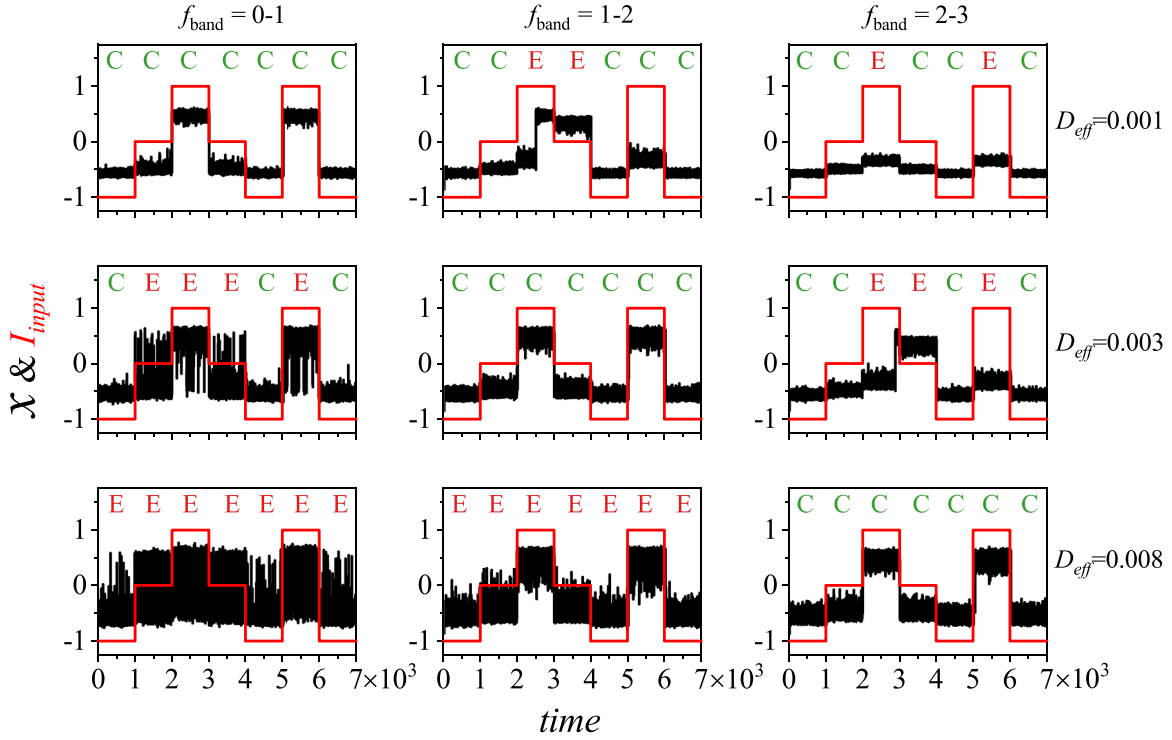
FIG. 7. The sampled time series of x (black lines) and I_{input} (red lines) for AND logic operations. E and C represent error and correct operations, respectively. From top panel to bottom panel, $D_{eff} = 0.001$ (top), 0.003 (middle), and 0.008 (bottom). From left panel to right panel: $f_{band} = 0 - 1$ (left), $f_{band} = 1 - 2$ (middle), $f_{band} = 2 - 3$ (right).

C. Modulation mechanisms of state transitions by high- and low-frequency components

Finally, we would like to explain the reasons for the superiority of low-pass filtered noise. As we have discussed in the model section, the effective potential well of the system is dynamically changed by the logical inputs. The two bistable states are axisymmetric with $x = 0$ in Fig. 1(b), so we can use the case of $I_{input} = 1$ as an example. To obtain reliable logic operations, the system needs to transition from the left (error) potential well to the right (correct) potential well before the measurement time T_0 ends. Figure 11(b) shows an example of a failed logic operation at $f_{max} = 0.01$. It can be seen that even if the driving force in the opposite direction (negative) is larger, it has a minimal effect on the system. This is due to the role of the highly nonlinear nature of the quadratic term in the potential function. What contributes to the transition is the
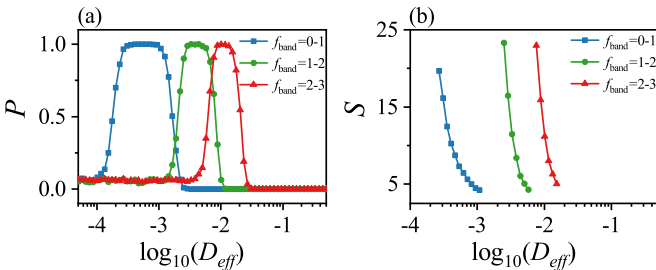
positive part of the driving force. Furthermore, for the system to complete a transition, the strength of the driving force must exceed a certain threshold and sustain for a certain duration.
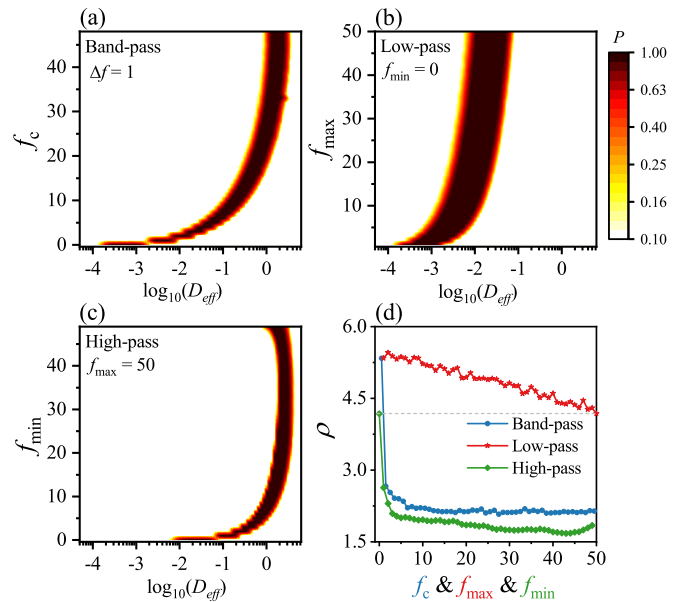

FIG. 9. The success probability P as a function of the parameter space (a) $(f_c \times D_{eff})$ for band-pass filtered noise; (b) $(f_{max} \times D_{eff})$ for low-pass filtered noise; (c) $(f_{min} \times D_{eff})$ for high-pass filtered noise; (d) dependence of the stability factor ρ on the cutoff frequency. ρ of Gaussian white noise is represented by the gray dash line for comparison.

FIG. 8. The (a) success probability P and (b) switching time S versus effective noise intensity D_{eff} with different frequency bands f_{band}.
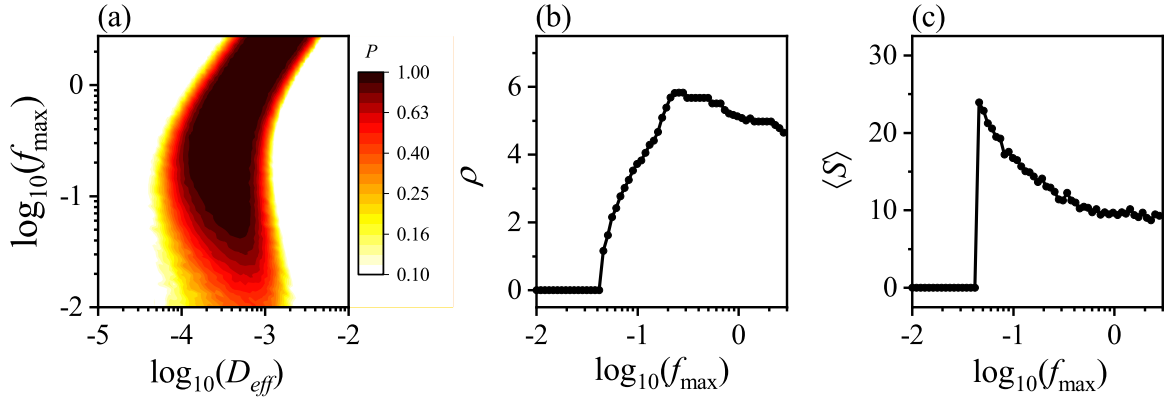
FIG. 10. Response of bistable systems to filtered noise on large timescales. (a) The success probability P as a function of the parameter space ($f_{max} \times D_{eff}$) for low-pass filtered noise. Dependence of the (b) stability factor ρ and (c) mean switching time $\langle S \rangle$ on f_{max} for low-pass filtered noise.

This can easily be verified in Fig. 11(c). Comparing the left and middle panels of Fig. 11(c), the duration can induce a state transition even if the strength of the driving force is the same. Furthermore, an increase in strength can also induce a state transition even if the duration of the driving force is the same [middle and right panels of Fig. 11(c)]. This suggests that state transitions require the cooperative effect of the two.

So far, we can understand why the stability of the logic operation varies nonmonotonically with f_{max}, driven by low-pass filter noise. When the timescale of the filtered noise is close to the measurement time (or transient process) T_0, the

probability of fluctuations with suitable intensity and duration is low. The duration of the driving force is also affected when high-frequency band noise is introduced excessively. Therefore, the most stable logic operation can be obtained for the system only if the timescale of the filtered noise is slightly larger than T_0. In addition, for the band-pass and high-pass cases, the part of the lower frequency band that is beneficial for the duration increase is filtered out. This is why the stability of the logic operation in the band-pass and low-pass cases is significantly lower than that of the noise source in Fig. 9(d).
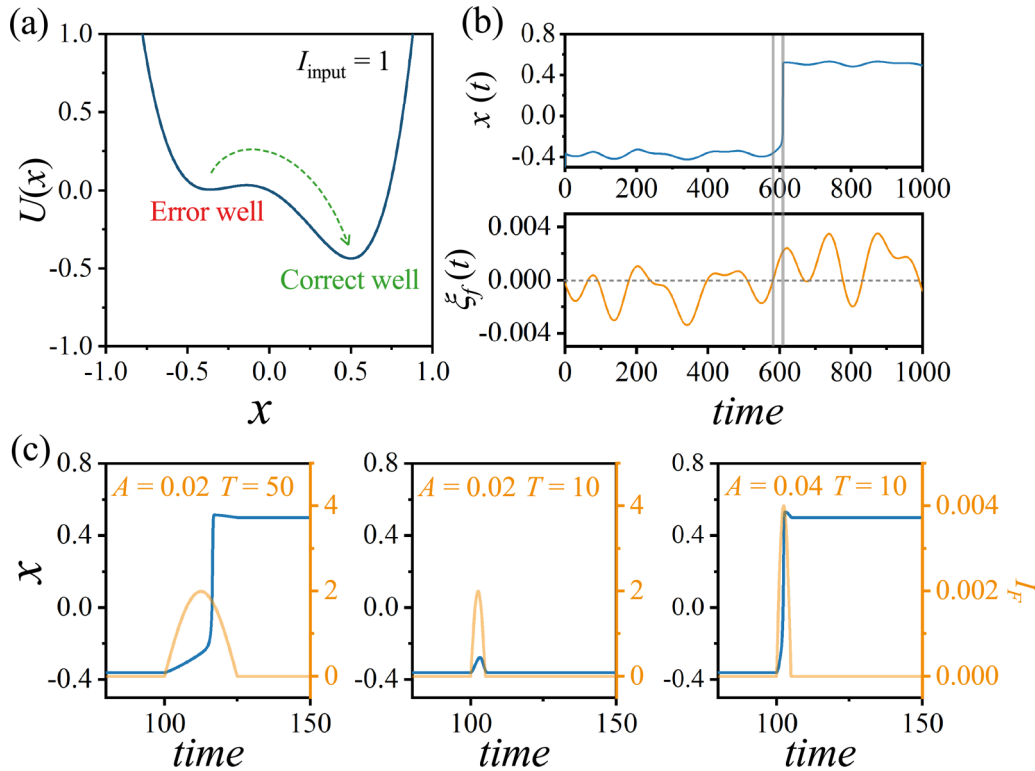

FIG. 11. Dynamical mechanisms for the effect of fast- and slow-scale driving forces on LSR. (a) Schematic representation of the desired state transition at $I_{input} = 1$. (b) Slow-scale filtering noise ($f_{min} = 0$, $f_{max} = 0.01$, $D_{eff} = 0.0005$) drives the system state to complete the desired transition. (c) Effect of half-cycle sinusoidal signals $I_F = A\sin(\frac{2\pi}{T}t)$ on state transitions.

IV. CONCLUSIONS

In this paper, we presented a simple and general theoretical background to explain the emergence of LSR in generalized bistable systems. We introduced dynamic logic inputs into the potential function to obtain a dynamic effective potential function. Based on the master equation approach of the two-state model, we solved analytically for the transition probability as a function of noise intensity and measurement time. The results were also compared with numerical simulations and quantitatively consistent conclusions were obtained. Furthermore, the mechanism of LSR can be understood by solving for the MPFT of the two-state transitions. The system can only obtain reliable logic operations if the MFPT of the desired transition is much smaller than the measurement time T_0 while the MFPT of the undesired transition is much larger than the calculation time interval T_{inter}. Therefore, the system can be continuously mapped to logic inputs only at moderate noise levels.

Furthermore, we proposed a way to drive LSR. Here, the filtered noise obtained by the FFT filtering method is considered as the driving force of the system. This is clearly different from previous studies in which the system was driven by noise [6–16], periodic signals [37], and chaotic signals [25,26]. Our results show that the occurrence of LSR depends on the cooperative effect of the intensity and the frequency characteristics of the filtered noise. In addition, the response speed of a logic device can be improved by appropriately increasing the level of filtering noise. We compared three types of filtering methods. It can be found that the stability of the filtered noise obtained by the band-pass and high-pass methods was much lower than that of the noise source due to the absence of the low-frequency part. Low-pass filtered noise is generally higher than the noise source. The underlying mechanisms are also discussed.

Bistable properties are widely found in natural systems such as nanomachines [9], gene regulation networks [13–15], nervous systems [38], etc. A recent study [16] using the bistability of neurons to achieve reliable logic devices expresses the advantages of high stability and low energy consumption. Our results can help us to understand the dynamical mechanism even though it is a four-dimensional dynamical model. Therefore, the obtained findings may provide a unique perspective for the design of more logic devices.

[1] L. Gammaitoni, Appl. Phys. Lett. **91**, 224104 (2007).

[2] L. Gammaitoni, P. Hänggi, P. Jung, and F. Marchesoni, Rev. Mod. Phys. **70**, 223 (1998)

[3] M. Löcher, D. Cigna, E. R. Hunt, G. A. Johnson, F. Marchesoni, L. Gammaitoni, M. E. Inchiosa, and A. R. Bulsara, Chaos **8**, 604 (1998).

[4] E. Simonotto, M. Riani, C. Seife, M. Roberts, J. Twitty, and F. Moss, Phys. Rev. Lett. **78**, 1186 (1997)

[5] D. Yu, G. W. Wang, Q. M. Ding, T. Y. Li, and Y. Jia, Chaos, Solitons Fractals **157**, 111929 (2022)

[6] K. Murali, S. Sinha, W. L. Ditto, and A. R. Bulsara, Phys. Rev. Lett. **102**, 104101 (2009).

[7] K. Murali, I. Rajamohamed, S. Sinha, W. L. Ditto, and A. R. Bulsara, Appl. Phys. Lett. **95**, 194102 (2009).

[8] L. Worschech, F. Hartmann, T. Y. Kim, S. Höfling, M. Kamp, A. Forchel, J. Ahopelto, I. Neri, A. Dari, and L. Gammaitoni, Appl. Phys. Lett. **96**, 042112 (2010)

[9] D. N. Guerra, A. R. Bulsara, W. L. Ditto, S. Sinha, K. Murali, and P. Mohanty, Nano Lett. **10**, 1168 (2010).

[10] K. P. Singh and S. Sinha, Phys. Rev. E **83**, 046219 (2011).

[11] S. Perrone, R. Vilaseca, and C. Masoller, Opt. Express **20**, 22692 (2012)

[12] S. Sinha, J. Cruz, T. Buhse, and P. Parmananda, Europhys. Lett. **86**, 60003 (2009).

[13] H. Ando, S. Sinha, R. Storni, and K. Aihara, Europhys. Lett. **93**, 50001 (2011).

[14] A. Dari, B. Kia, A. R. Bulsara, and W. Ditto, Europhys. Lett. **93**, 18001 (2011).

[15] E. H. Hellen, S. K. Dana, J. Kurths, E. Kehler, and S. Sinha, PLoS ONE **8**, e76032 (2013).

[16] D. Yu, L. J. Yang, X. Zhan, Z. Y. Fu, and Y. Jia, Nonlinear Dyn. **111**, 6757 (2023).

[17] G. Cheng, W. Liu, R. Gui, and Y. Yao, Chaos Solitons Fractals **131**, 109514 (2020).

[18] H. Zhang, T. Yang, W. Xu, and Y. Xu, Nonlinear Dyn. **76**, 649 (2014).

[19] Y. G. Yao, Pramana **95**, 77 (2021).

[20] N. Wang and A. G. Song, Phys. Lett. A **378**, 1588 (2014).

[21] Manaoj Aravind V, K. Murali, and S. Sinha, Phys. Lett. A **382**, 1581 (2018).

[22] Y. G. Yao, Chin. Phys. B **30**, 060503 (2021).

[23] M. Aravind, P. Parmananda, and S. Sinha, Phys. Rev. E **104**, 064207 (2021).

[24] N. Wang and A. G. Song, Neurocomputing **155**, 80 (2015).

[25] Y. G. Yao and J. Ma, Int. J. Bifurc. Chaos **30**, 2050196 (2020).

[26] Y. G. Yao, J. Ma, R. Gui, and G. H. Cheng, Chaos **31**, 023103 (2021).

[27] M. Das and H. Kantz, Phys. Rev. E **100**, 032108 (2019).

[28] K. Murali, W. L. Ditto, and S. Sinha, Phys. Rev. Appl. **18**, 014061 (2022).

[29] B. McNamara and K. Wiesenfeld, Phys. Rev. A **39**, 4854 (1989)

[30] R. L. Stratonovich, *Topics in the Theory of Random Noise* (Gordon and Breach, New York, 1963), Vol. 1.

[31] K. Lindenberg and B. J. West, J. Stat. Phys. **42**, 201 (1986).

[32] J. Masoliver, B. J. West, and K. Lindenberg, Phys. Rev. A **35**, 3086 (1987).

[33] E. Guardia and M. San Miguel, Phys. Lett. A **109**, 9 (1985).

[34] P. Hänggi, F. Marchesoni, and P. Grigolini, Z. Phys. B **56**, 333 (1984).

[35] R. F. Fox, Phys. Rev. A **33**, 467 (1986).

[36] R. F. Fox, I. R. Gatland, R. Roy, and G. Vemuri, Phys. Rev. A **38**, 5938 (1988).

[37] A. Gupta, A. Sohane, V. Kohar, K. Murali, and S. Sinha, Phys. Rev. E **84**, 055201(R) (2011).

[38] D. Yu, L. L. Lu, G. W. Wang, L. J. Yang, and Y. Jia, Chaos, Solitons Fractals **147**, 111000 (2021).